Experimental and Molecular Pathology 91 (2011) 400–410

Contents lists available at ScienceDirect

Experimental and Molecular Pathology

journal homepage: www.elsevier.com/locate/yexmp

Small molecule inhibitors of the host cell COX/AREG/EGFR/ERK pathway attenuate cytomegalovirus-induced pathogenesis

Michael Melnick [a,*], George Abichaker [a], Khine Htet [a], Parish Sedghizadeh [b], Tina Jaskoll [a]

[a] Laboratory for Developmental Genetics, USC, Los Angeles, CA, USA
[b] Oral and Maxillofacial Pathology, Division of Diagnostic Sciences, USC, Los Angeles, CA, USA

ARTICLE INFO

Article history:
Received 14 April 2011
Available online 1 May 2011

Keywords:
Cytomegalovirus
CMV-induced pathology
COX-2
Amphiregulin
EGF receptor
ERK

ABSTRACT

As with other herpesviruses, human cytomegalovirus (hCMV) has the ability to establish lifelong persistence and latent infection following primary exposure, salivary glands (SMGs) being the primary site of both. In the immunocompromised patient, hCMV is a common cause of opportunistic infections, and subsequent morbidity and mortality. Elucidating the molecular pathogenesis of CMV-induced disease is critical to the development of more effective and safer drug therapies. In the present study, we used a novel mouse postnatal SMG organ culture model of mCMV-induced dysplasia to investigate a candidate signaling network suggested by our prior studies (COX-2/AREG/EGFR/ERK). The objective was to employ small molecule inhibitors to target several key steps in the autocrine loop, and in this way ameliorate pathology. Our results indicate that upregulation of ERK phosphorylation is necessary for initial mCMV-induced pathogenesis, and that ErbB receptor family phosphorylation and downstream signaling are highly relevant targets for drug discovery.

Introduction

Nearly a century ago, pathologists reported that postmortem tissue examination of infants less than 1 year of age often revealed inclusion bodies in submandibular salivary glands (SMGs) and, less frequently, in liver, lung, kidney, and thyroid. The large cells ("cytomegalia") were found in acini and ducts of affected SMGs and the ducts were often dilated. By the 1950s, human cytomegalovirus (hCMV), a prototypical β-herpesvirus, was isolated and it became apparent that hCMV infection was common, 50–95% of adults being seropositive.

hCMV primary, recurrent and secondary infections are associated with variant adverse consequences, from asymptomatic viruria in immunocompetent hosts to serious congenital disorders (deafness, blindness, mental retardation) in newborns, infants, and toddlers. Further, hCMV is a common cause of frequent opportunistic infections in the immunocompromised patient (Kim et al., 2010; Mori and Kato, 2010), a significant contributing factor to morbidity and mortality. For example, in patients undergoing hematopoietic stem cell transplantation or receiving immunosuppressive chemotherapy, the risk of hCMV infection is 20–30% (Yahav et al., 2009).

As with other herpesviruses, hCMV has the ability to establish lifelong persistence and latent infection following primary exposure (Nichols and Boeckh, 2000), salivary glands being the primary site of both (Wagner et al., 1996; Nichols and Boeckh, 2000). hCMV shed in saliva from infected salivary glands are a key source for the etiology of oral and systematic disease in immunocompromised patients (Correia-Silva et al., 2007, 2010). Clearly, halting hCMV replication and survival in the salivary gland is key to eliminating hCMV oral infection and transmission. To date, there has been very limited success in developing an hCMV vaccine. Alternatively, four drugs have been licensed to treat adult hCMV infection, with intravenous ganciclovir being the treatment of choice (Schleiss and Choo, 2006; Andrei et al., 2008; Cheeran et al., 2009). Each of these compounds has significant toxicities that limit their use. Thus, there is an urgent need to develop new anti-CMV therapies.

Strict CMV species-specificity has hindered the study of hCMV in animal models. Nevertheless, since mouse CMV (mCMV) has many features in common with hCMV, and mCMV infection of mice resembles its human counterpart with respect to pathogenesis, the mouse animal model (in vitro and in vivo) has been extensively used to understand the pathogenesis of acute, latent, and recurrent infections (e.g. Reynolds et al., 1993; Lagenaur et al., 1994; Schmader et al., 1995; Krmpotic et al., 2003; Melnick et al., 2006; Pilgrim et al., 2007; Jaskoll et al., 2008a, 2008b; Bai et al., 2008; Kasman et al., 2009). As with humans, the SMG is the major target organ for mCMV replication in the infected mouse. Some insight into the cell and molecular pathogenesis of mCMV-infected SMGs has emerged from our study of mCMV-infected fetal SMGs (Melnick et al., 2006). CMV, in its intracellular habitat, exploits and subverts a variety of host cell

* Corresponding author at: Laboratory for Developmental Genetics, University of Southern California, 925 W 34th Street, DEN 4264, MC-0641, Los Angeles, CA 90089-0641 USA. Fax: +1 213 740 7560.
E-mail addresses: mmelnick@usc.edu (M. Melnick), abichake@usc.edu (G. Abichaker), khtet@usc.edu (K. Htet), sedghiza@usc.edu (P. Sedghizadeh), tjaskoll@usc.edu (T. Jaskoll).

0014-4800/$ – see front matter © 2011 Elsevier Inc. All rights reserved.
doi:10.1016/j.yexmp.2011.04.014

factors for survival and growth in an otherwise hostile cellular environment (Melnick et al., 2006; Sanchez and Spector, 2008). Studies of mCMV-infected fetal SMGs suggest that prominent among these are receptor kinase pathways and activated NFκB target gene pathways (Melnick et al., 2006). These findings recommend a newly emerging drug discovery paradigm that identifies and targets hijacked host factors, in contrast to canonical pathogen-targeting strategies (Andrei et al., 2008; Schwegmann and Brombacher, 2008).

Though cellular signaling pathways may seem obvious targets for therapeutic intervention, such strategies are complicated by the fundamental problem of interrelating genomics, proteomics, and phenotype in complex disease. To approach this conundrum, we have recently developed a novel mouse postnatal SMG organ culture model of mCMV-induced pathology (Jaskoll et al., 2011). This CMV-induced "sentinel neoplasia" model provides an ideal system for investigating virally-induced dysregulation of multiple host cell signaling pathways, focusing on a network of interactions between genes and pathology. Moreover, since the three dimensional associations between acinar, ductal and stromal cells are maintained, this postnatal SMG organ culture permits delineation of the cell-specific localization of important molecules with progressive infection and identifies changes in pathway components in a variety of cell types, thus providing evidence for the physiologic relevance of those components.

In the present study, we investigated a signaling network previously suggested in studies of CMV-induced fetal SMG dysplasia (Melnick et al., 2006), hypothesizing that this network would be highly relevant to postnatal CMV-induced tumorigenesis (Jaskoll et al., 2011). The objective of this study was to use small molecule inhibitors to target several key steps in the cognate COX-2/AREG/EGFR/ERK autocrine loop, and in this way ameliorate pathology. Our results strongly indicate that the upregulation of ERK phosphorylation is necessary for initial mCMV-induced postnatal SMG pathogenesis, and that ErbB-family phosphorylation and downstream signaling are highly relevant targets for drug therapy.

Materials and methods

Animals

Timed pregnant inbred C57/BL6 female mice (Charles River, Wilmington, MA) were purchased from Charles River (Wilmington, MA) [plug day = day 0 of gestation] and newborn mice were harvested as previously described (Melnick et al., 2006, 2009). All protocols involving mice were approved by the Institutional Animal Care and Use Committee (USC, Los Angeles, CA).

Organ culture

Newborn SMGs were dissected and cultured for 6 or 12 days using a modified Trowell method and BGJb medium (Invitrogen Corporation, Carlsbad, CA) supplemented with 10% fetal calf serum (FCS), 0.5 mg ascorbic acid/ml and 50 units/ml penicillin/streptomycin (Invitrogen Corporation), pH 7.2 as previously described (Melnick et al., 2006). For mCMV infection, SMGs were incubated with 1×10^{-5} plaque-forming units (PFU)/ml of *lacZ*-tagged mCMV RM427+ in BGJb on day 0 for 24 h and then cultured in virus-free media for a total of 6 or 12 days in culture; controls consisted of SMGs cultured in control medium for the entire period. SMGs were collected and processed for hematoxylin and eosin histology, qRT-PCR, Western blot analysis, immunolocalization, or cell proliferation (PCNA) analysis. For histology, immmunolocalization, and PCNA analysis, SMGs were fixed for 4 h in Carnoy's fixative at 4 °C or overnight in 10% neutral buffered formalin at room temperature, embedded in paraffin, serially-sectioned at 8 μm and stained as previously described (Melnick et al., 2006).

Cell proliferation assay

The cell-specific localization of PCNA (proliferating cell nuclear antigen) was determined using the Zymed mouse PCNA kit (Invitrogen Corporation) and counterstained with hematoxylin and eosin essentially as previously described (Melnick et al., 2006). In this set of experiments, the cytoplasm appears blue and PCNA-positive nuclei appear dark brown. For cell proliferation analysis, 3–8 SMGs per treatment per day were analyzed.

Quantitative RT-PCR

For analysis of gene expression, quantitative RT-PCR (qRT-PCR) was conducted as previously described (Melnick et al., 2006). We performed quantitative RT-PCR on NB + 6 control and mCMV-infected SMG samples; each sample consisted of 3–4 pooled explants. RNA was extracted and 1 μg RNA was reverse transcribed into first strand cDNA using ReactionReady™ First Strand cDNA Synthesis Kit: C-01 for reverse transcription (SABiosciences, Frederick, MD). The primer sets used were prevalidated to give single amplicons and purchased from SABiosciences (Frederick, MD): AREG (PPM02976A); Cox 2 (Ptgs2; Cat # PPM03647A); EGFR (PPM03714A); ERK1 (Mapk3; Cat. # PPM03585A); PCNA (Cat. # PPM03456A). Primers were used at a concentration of 0.4 μM. The cycling parameters were 95 °C, 15 min; 40 cycles of (95 °C, 15 s; 55 °C, 30–40 s and 72 °C, 30 s). Specificity of the reactions was determined by subsequent melting curve analysis. RT-PCRs of RNA (not reverse transcribed) were used as negative controls. GAPDH was used to control for equal cDNA inputs and the levels of PCR product were expressed as a function of GAPDH. The relative fold changes of gene expression between the gene of interest and GAPDH, or between the NB + 6 control and mCMV-infected SMGs, were calculated by the $2^{-\Delta\Delta CT}$ method.

Immunolocalization

Cultured SMGs were fixed for 4 h in Carnoy's fixative at 4 °C, embedded in low melting point paraplast, serially-sectioned at 8 μm and immunostaining was conducted as previously described (Melnick et al., 2006, 2009) using the following polyclonal rabbit antibodies: pERK1/2 (Thr202/Tyr204), pEGFR (Tyr1173), Amphiregulin (Santa Cruz Biotechnology, Inc, Santa Cruz, CA) and Cox-2 (Cayman Chemicals, Ann Arbor, MI). Sections were incubated with biotin-labeled rabbit IgG (Fab fragment)(MP Biomedical, Aurora, OH) and then with Alexa-Fluor-labeled streptavidin (Invitrogen Corporation). Nuclei were counterstained with DAPI (Invitrogen Corporation). Negative controls were performed in parallel under identical conditions and consisted of sections incubated without primary antibodies. For each treatment group, 5–10 SMGs per day were analyzed.

Western blot analysis

NB + 6 uninfected (control), mCMV-infected, DCF-treated mCMV-infected, and GEF-treated mCMV-infected SMGs were collected; each independent sample consisted of 3–4 explants per group. Proteins (25–35 μg) were separated by SDS-PAGE gels and transferred to a PVDF membrane, and the membranes were subjected to chemiluminescence detection (ECL) according to the manufacturer's instructions (Thermo-Scientific, Rockford, IL) as previously described (Melnick et al., 2006). The following polyclonal antibodies were used: pERK1/2 (Thr202/Tyr204) (Cell Signaling Technology); Amphiregulin, Cox-2, and β-actin (Santa Cruz Biotechnology). Data was quantitated by using the ImageJ image analysis software (NIH) and normalized to the level of β-actin expression in each sample.

Proteome RTK antibody array

To determine if mCMV infection altered the relative level of tyrosine phosphorylation of mouse receptor tyrosine kinases (RTKs), we used the Mouse Phospho-RTK Array Proteome Profiler Antibodies Array (R & D Systems, Minneapolis, MN) according to manufacturer's directions. This array allows for the parallel screening of relative levels of tyrosine phosphorylation in 39 different mouse RTKs. NB + 6 mCMV-infected, and GEF-treated, mCMV-infected SMGs were collected; each independent sample consisted of 3–4 explants. Proteins were extracted, 120–125 mg protein per sample was added to each array, and proteins were viewed using the ECL system (Amersham). Array images were collected from 30 s to 10 min exposures to X-ray film. Positive control spots were used to align the transparency overlay to enable the identification of specific phosphorylated RTKs. The relative level of phospho-RTK was quantitated using the ImageJ image analysis software (NIH).

Interruption studies

We conducted 3 sets of interruption studies using small molecule inhibitors. For all small molecule inhibitors, we first conducted dose response studies to determine the optimal, nontoxic dose that substantially precludes mCMV-induced pathology in cultured NB SMG organs. After determining the optimal nontoxic dose, we then cultured mCMV-infected or uninfected NB SMGs in the presence or absence of treatment for a total of 6 days and SMGs were collected and analyzed. (1) DCF: To interrupt COX-2 signaling, we used diclofeneac sodium salt (DCF) (Sigma-Alrich Corp, St. Louis, MO), a nonselective COX inhibitor which is mostly a COX-2 inhibitor. To determine the optimal nontoxic dose of DCF that precludes mCMV-induced pathology, NB SMGs were infected with 1×10^5 PFU/ml mCMV for 24 h in the presence or absence of 10 μM, 1 μM, or 100 nM DCF, and then cultured in control medium with or without DCF for a total of 6 days; controls consisted of glands cultured in control medium or control medium + DCF for the entire 6 days. In this experiment, 4–6 explants per treatment were analyzed using routine hematoxylin and eosin histology. Based on this dose–response experiment, we then used 1 μM DCF in all subsequent experiments. (2) GEF: To interrupt EGFR signaling, we used gefitinib (GEF) (Selleck Chemicals LLC, Houston, TX), a small molecule inhibitor which blocks the binding of ATP to the intracellular TK domain of EGFR to inhibit EGFR signaling. To determine the optimal nontoxic dose of GEF that precludes mCMV-induced pathology, NB SMGs were infected with 1×10^5 PFU/ml mCMV for 24 h in the presence or absence of 100 μM, 10 μM, 1 μM, or 100 nM GEF, and then cultured in control medium with or without GEF for a total of 6 days; controls consisted of glands cultured in control medium or control medium + GEF for the entire 6 days. In this experiment, 4–8 explants per treatment were analyzed using routine hematoxylin and eosin histology. Based on this dose response study, we then used 10 μM GEF in all subsequent experiments. (3) U0126: To interrupt ERK1/2 signaling, we used U0126 (EMD Chemicals, Inc, Gibbstown, NJ), a potent and specific inhibitor of MEK-mediated ERK1 and ERK2 phosphorylation. To determine the optimal nontoxic dose of U026 that precludes mCMV-induced pathology, NB SMGs were infected with 1×10^5 PFU/ml mCMV for 24 h in the presence or absence of 10 μM, 50 μM, or 100 μM U0126 and then cultured in control medium with or without U0126 for a total of 6 days; controls consisted of glands cultured in control medium or control medium + U0126 for the entire 6 days. In this experiment, 4–6 explants per treatment were analyzed using routine hematoxylin and eosin histology. Based on this experiment, we used 10 μM U0126 in all subsequent experiments.

Probabilistic neural network (PNN) analysis

We used PNN analyses to determine the contribution of individual cognate genes to the discrimination between experimental groups with 100% sensitivity and specificity. As such, PNN analyses identify the relative importance (0–1, with 0 being of no relative importance and 1 being relatively most important) of specific gene expression changes that discriminate between phenotypes. It is the contextual change in expression, not the direction of change that is important in defining the molecular phenotype. The foundational algorithm we used is based upon the work of Specht and colleagues (Chen, 1996; Specht, 1988; Specht and Shapiro, 1991).The proprietary software designed by Ward Systems Group (Frederick, MD) formulates Specht's procedure around a genetic algorithm (Goldberg, 1989). A genetic algorithm is a computational method modeled on biologic evolutionary processes that can be used to find the optimum solution to a problem that may have many solutions (Holland, 1975). These algorithms have been found to be very powerful in solving optimization problems that appear to be difficult or unsolvable by traditional methods. They use a minimum of information about the problem and they only require a quantitative estimation of the quality of a possible solution. This makes genetic algorithms easy to use and applicable to most optimization problems.

Statistical analysis

Significant differences between mCMV-infected and control SMGs, as well as between mCMV and mCMV + treatment SMGs, were determined by student *t*-test, with $\alpha = 0.05$ and the null hypothesis of $R = 1$. The calculated expression ratios (Rs) were log or arcsin transformed prior to analysis.

Results

The overarching paradigm of this research is to identify molecular targets for modulating phenotypic outcome to preclude or treat disease. Critical to this task is the ability to discern patterns of covariation related to molecular, physiologic, and histologic phenotypes. Simply, we must be able to relate measurements and localization of RNAs and proteins (input) to a well-defined phenotype (output). Thus, we employed an in vitro SMG organ culture strategy shown to induce cellular pathology which resembles secretory glandular neoplasia (Melnick et al., 2006; Jaskoll et al., 2011).

CMV-induced histopathology

Newborn (NB) mouse SMGs were cultured with 1×10^5 PFU/ml mCMV for 24 h and maintained for 6 or 12 days; controls consisted of NB SMGs cultured for identical periods in control medium. mCMV infection results in a severely dysplastic phenotype compared to controls (compare Fig. 1B to A, D to C). In mCMV-infected SMGs, ductal epithelia are hyperplastic, dysplastic and pseudostratified in some areas, resulting in an overall architecture that is poorly organized and dysmorphic. Epithelial cells are hyperchromatic and have increased nuclear-to-cytoplasmic ratios, prominent nuclei and nucleoli, nuclear indentations perpendicular to the nuclear membrane, loss of cytoplasmic eosinophilic granularity and occasional mitotic figures. Often ductal lumina are markedly dilated, with lumina containing mucinous and cellular debris. The stroma is abnormally hypercelluar, resulting in a loss or attenuation of the fibromyxoid stroma. Stromal cellularity is characterized by clusters of basophilic, megaloblastic, pleomorphic cells with high nuclear-to-cytoplasmic ratios and frequent “owl's eye” inclusion bodies. By day 12 of culture, there is a distinctly new population of small eosinophilic stromal cells with oncocytic-like stromal metaplasia. At many pro-acini, there appears an admixing or comingling of basophilic mesenchymal cells and epithelial pro-acinar cells (Fig. 1D). In both NB + 6 and NB + 12 mCMV-infected SMGs, the hypercellular, cytomegalic stroma displays frequent PCNA-positive nuclei, a marker of cells in early G_1 and S phases of the cell cycle (compare 1 F to 1E, 1 H to 1 G).

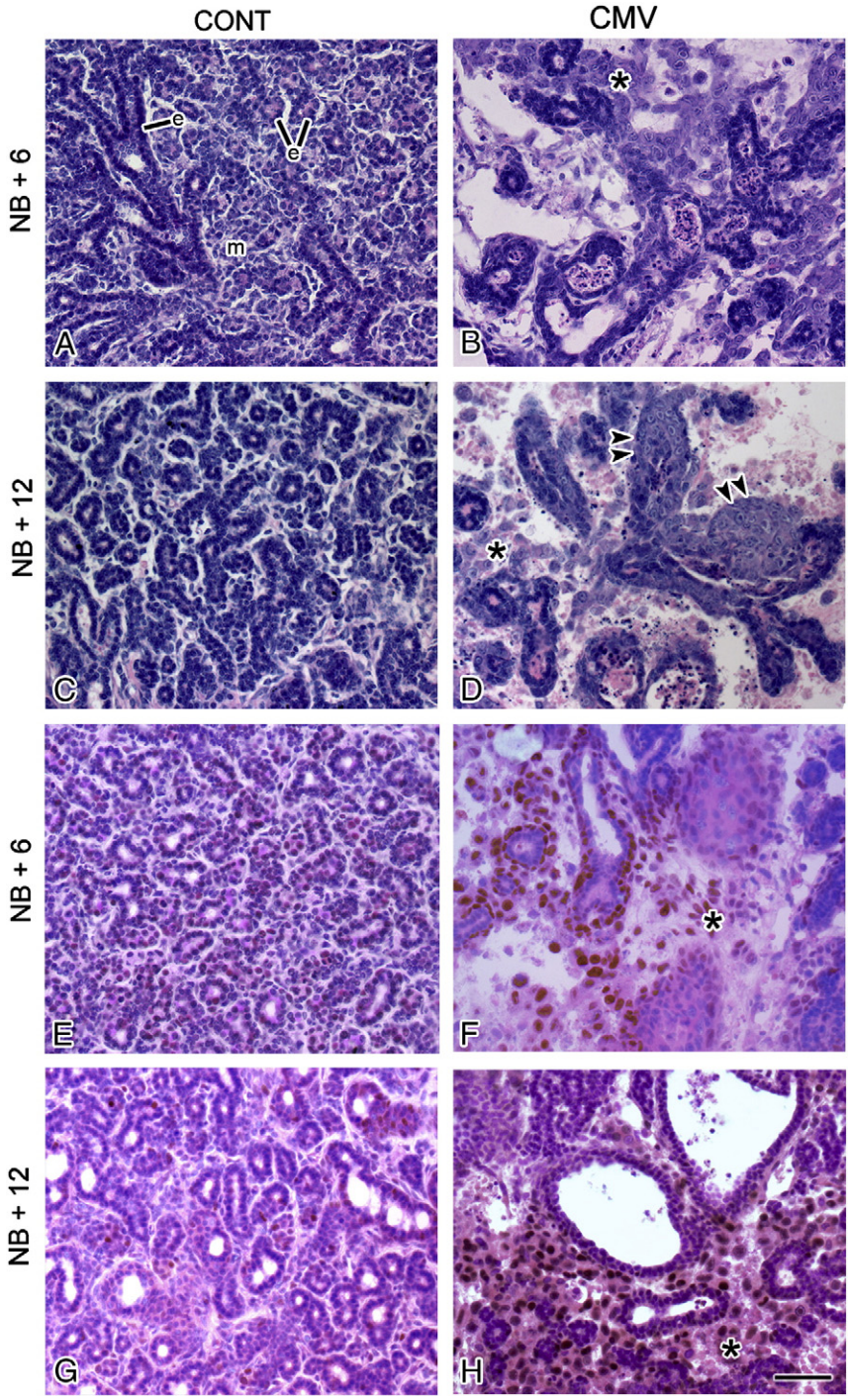

Fig. 1. mCMV-infected newborn SMGs exhibit a tumor-like histopathology and qualitative changes in cell proliferation. A–D. Histological analysis of control (A, C) and mCMV-infected (B, D) newborn SMGs cultured for 6 days (NB + 6) and 12 days (NB + 12). Control SMGs (A, C) are characterized by epithelial (e) ducts and pro-acini with distinct lumina being surrounded by a single layer of cuboidal cells; the epithelial component is embedded in compacted mesenchyme (m). mCMV-infected SMGs cultured for 6 days (B) are severely dysmorphic, characterized by marked decrease in branching epithelia and abnormal ducts composed of hyperplastic and pseudostratified epithelia surrounding severely dilated lumina. Some ductal lumina appear cystic and contain mucinous and cellular debris within the lumen. These abnormal epithelial structures are embedded in a hypercellular stroma (*) composed primarily of giant basophilic round cells and, to a lesser degree, smaller eosinophilic cells. In NB + 12 mCMV-infected SMGs (D), the stromal cells are composed of 2 distinct cell types: large basophilic round cells and smaller eosinophilic cells. There appears to be an admixing of the dual population of cells comprising an aggregation of the basophilic stromal cells and the pro-acinar cells (arrowheads). These abnormal cells frequently exhibit viral inclusion bodies. E–H. The cell-specific localization of proliferating cell nuclear antigen (PCNA) in control (E, G) and mCMV-infected (F, H) cultured for 6 days (NB + 6) and 12 days (NB + 12).E–H. In controls (E, G), PCNA-positive nuclei are seen in ductal and pro-acinar epithelia and infrequently in the mesenchyme on day 6 (E); by day 12 (G), there is a marked decrease in PCNA-positive nuclei. In mCMV-infected SMGs (F, G), there is a marked increase in PCNA-positive nuclei as compared to controls (compare F to E and H to G). PCNA-positive nuclei are found primarily in the cytomegalic, hypercellular stromal cells and is relatively absent from epithelia. Bar scale: 40 μm.

CMV-induced molecular pathology

Prior work in our laboratory demonstrated that mCMV infection of SMGs upregulates host cell NFκB activation which in turn upregulates the COX-2/PGE2/EP4 pathway (Melnick et al., 2006). Other studies have shown: 1) PGE2/EP4 can induce amphiregulin (AREG) and thereby activate EGFR signaling and cell proliferation; 2) activated EGFR positively regulates COX-2/PGE2/EP4/AREG pathway; and 3)

activated ERK negatively regulates ERK activation (phosphorylation) (Liu et al., 2007; Yonesaka et al., 2008; Sturm et al., 2010). All these relationships can be visualized in a systems genetics network of interactions between gene functions and phenotypic traits, as well as between gene functions themselves (Fig. 2A). A priori predictions that derive from this network were tested with CMV and small molecule inhibitor (DCF, GEF, U0126) exposures as single-factor perturbations (Fig. 2A).

As above, NB mouse SMGs were cultured with or without 1×10^5 PFU/ml mCMV for 24 h and maintained in culture of a total of 6 days. Quantitative RT-PCR (qRT-PCR) reveals an 80-fold increase in COX-2 transcript, a 4-fold increase in AREG transcript, a 30% increase in PCNA transcript, and a 30% decline in ERK1 transcript (Table 1). Using a neural network learning method, our unbiased optimization algorithm demonstrates that with the transcript levels of only 4 genes (COX-2, AREG, ERK1, PCNA), a SMG organ can be classified as CMV-exposed or not with 100% sensitivity and 100% specificity; not surprisingly, COX-2 and AREG transcription are relatively more important than are PCNA and ERK1 (Fig. 2B).

Quantitative protein analysis provides additional support to the model. COX-2 shows a 6-fold increase with mCMV infection (Table 1, Fig. 3A); COX-2 immunolocalizes to the cytomegalic stromal cells, and is almost unseen in uninfected control SMGs (Fig. 3D, J). AREG exhibits a 2-fold increase with mCMV infection (Table 1; Fig. 3B); AREG immunolocalizes to the cytomegalic stromal cells and on the apical surfaces of epithelial lumina, but in controls, AREG is only found on epithelial cell membranes (Fig. 3E, K). Phospho-ERK1/2 (pERK) shows a 2 fold increase with mCMV infection (Table 1; Fig. 3C); pERK immunolocalizes nearly exclusively to cytomegalic stromal cells, and is rarely seen in uninfected controls (Fig. 3F, L). As anticipated, a negative feedback precludes correspondence between ERK transcript levels and that of activated pERK protein. Significant upregulation of pERK is, of course, a critical expectation of the proposed network, as is the significant upregulation of COX-2 and AREG proteins (Fig. 2A).

Table 1
mCMV exposure: transcript and protein measures.

	mRNA				Protein		
	R	η	P		R	η	P
COX-2	80.7	0.71	<0.01	COX-2	6.1	0.61	<0.01
AREG	4.2	0.49	<0.01	AREG	2.0	0.21	<0.05
ERK1	0.7	0.16	<0.001	pERK	2.0	0.38	<0.01
PCNA	1.3	0.21	<0.002	PCNA	**	–	–

R = mean relative expression ratio = mCMV/control (comparisons: n = 9).
η = gene expression noise (0 → 1) = S_R/R (where S_R = standard deviation of R).
** see Fig. 1E, F.

COX-2 inhibition

One a priori prediction of the proposed network (Fig. 2A) is that inhibition of COX-2 should result in normal levels of AREG and pERK1/2, and attenuated pathology, in mCMV-infected SMGs. Diclofenac sodium (DCF) is a nonselective COX inhibitor, though it is mostly COX-2 selective. In this experiment, NB SMGs were infected with 1×10^5 PFU/ml mCMV for 24 h in the presence or absence of 1 μM DCF, and then cultured in control medium with or without DCF for a total of 6 days. Controls consisted of glands cultured in control medium or control medium + DCF for the entire 6 days; DCF-treated and untreated control SMGs exhibit a similar phenotype (compare Fig. 4B to A). All glands were collected on day 6 (NB + 6) for routine H&E histology and Western blot analysis (Fig. 4). With 1 μM DCF

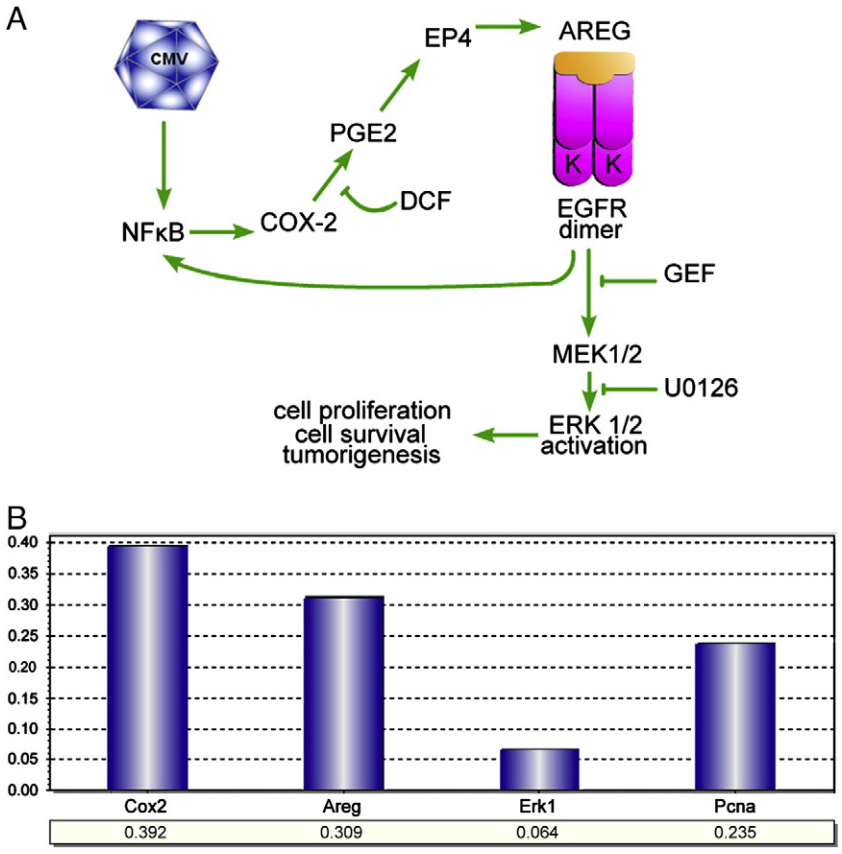

Fig. 2. A. Systems genetics network model of interactions between COX-2/AREG/EGFR/ERK and CMV-induced pathology. B. Neural network analysis was used to determine the contribution of relevant genes to the unbiased classification of NB + 6 SMG organs as either mCMV-infected or uninfected (control) with 100% sensitivity and 100% specificity.

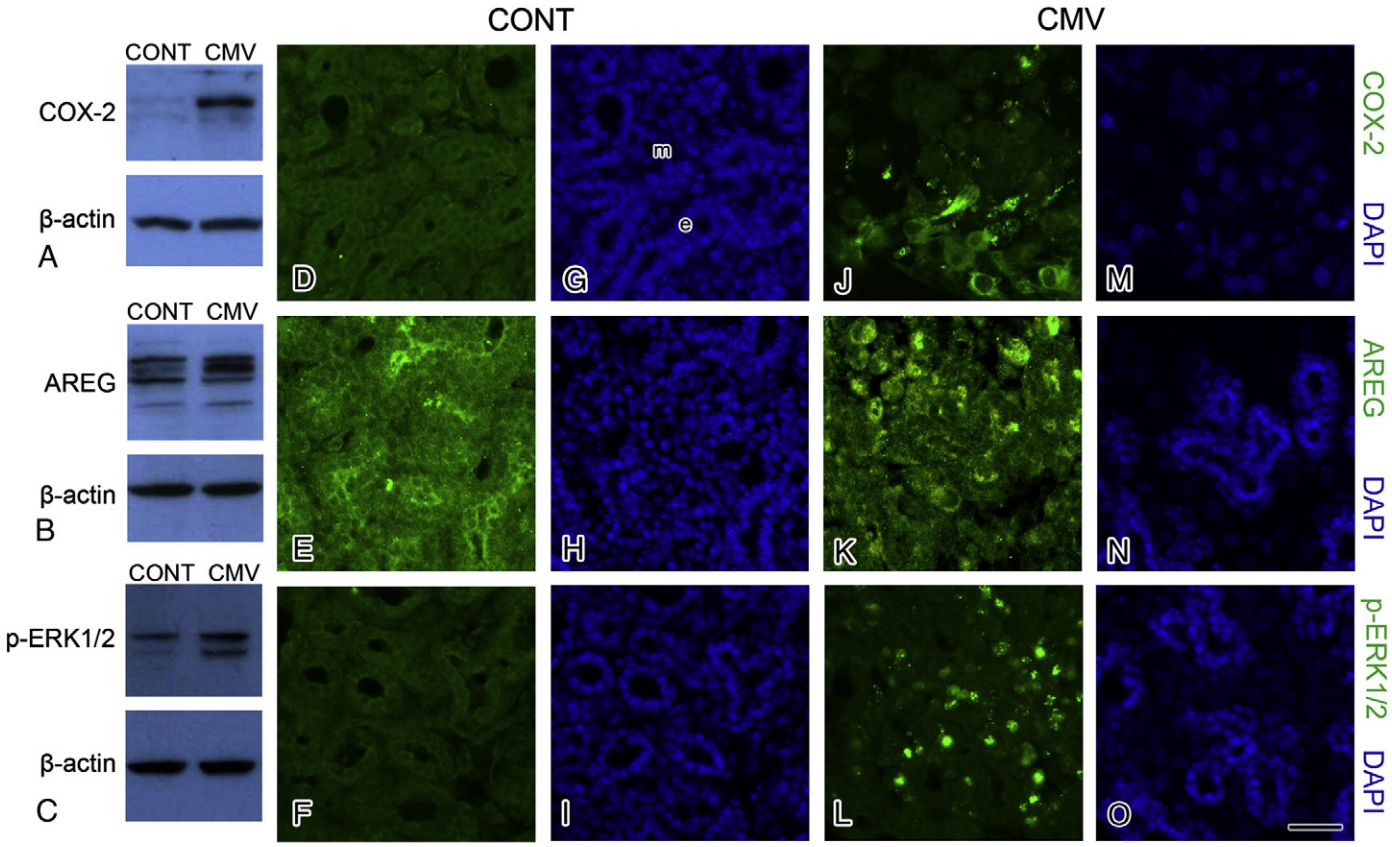

Fig. 3. CMV induces a marked increase in COX-2, AREG and activated ERK1/2 protein expression in NB + 6 SMGs. A–C. Western blot analysis demonstrates that mCMV induces a significant upregulation of COX-2 (A), AREG (B), pERK1/2 (C) compared to control (see Table 1). D–O. Immunolocalization of COX-2 (D, J), AREG (E, K), and phosphorylated ERK1/2 (pERK) (F, L). DAPI was used to counterstain nuclei (G–I, M–O) in sections shown in D–F and J–L. With mCMV infection, there is a notable increase in immunodetectable COX-2 (J), AREG (K) and phospho-ERK1/2 (L) as compared to controls (compare J to D, K to E, L to F). Note that COX-2, AREG and phospho-ERK1/2 proteins are primarily found in cytomegalic stromal cells. Bar scale: D–O, 15 μm.

treatment of mCMV-infected SMGs, there is considerable "rescue" of the viral-induced pathology. There is a substantial increase in ductal and acinar epithelia, with normal-sized lumina, resulting in a normal epithelial phenotype (compare Fig. 4D to C). Although the stroma is much improved in appearance, there still remains a small, but widespread, amount of basophilic hypercellularity (Fig. 4D); there are few, if any, inclusion bodies. The attenuated histologic outcome of COX-2 inhibited, mCMV-infected, glands as compared to COX-2 uninhibited is coincident with a significant decline in AREG ($R = 0.71$, $n = 9$, $p < 0.001$) and pERK1/2 ($R = 0.68$, $n = 9$, $P < 0.05$) (Fig. 4E, F), both of which are downstream of COX-2 (Fig. 2A).

EGFR inhibition

Another a priori prediction of the proposed network (Fig. 2A) is that inhibition of EGFR phosphorylation should result in normal levels of pERK 1/2 and COX-2, and attenuated pathology, in mCMV-infected SMGs. Since many ligands other than AREG bind to EGFR (e.g. EGF, TGFα, Epiregulin, Heparin-binding EGF, Betacellulin), one might reasonably expect a greater inhibition of pERK1/2 and a greater attenuation of pathology than that seen with COX-2 inhibition.

Systems analysis of the EGFR pathway has been important to targeted drug discovery (see review, Lurje and Lenz, 2009). To wit, gefitinib (GEF) blocks the binding of ATP to the intracellular TK domain of EGFR and thus inhibits downstream ERK1/2 activation and cell proliferation, as well as promotes cell cycle arrest at the G_1-S boundary and apoptosis (Yonesaka et al., 2008; Favoni et al., 2010).

In this experiment, NB SMGs were infected with 1×10^5 PFU/ml mCMV for 24 h in the presence or absence of 10 μM GEF and then cultured in control medium with or without GEF for a total of 6 days. Controls consisted of SMGs cultured in control medium alone or control medium + GEF for the entire 6 day period; similar phenotypes were seen in GEF treated and untreated control SMGs (data not shown). All glands were collected on day 6 (NB + 6) for routine H & E histology and immunohistochemistry (Fig. 5), as well as Western blot analysis. With 10 μM GEF treatment of mCMV-infected SMGs, the attenuation of the pathology is even more striking than with DCF, with normal pro-acinar and canalicular epithelial cell structure and organization, as well as the presence of a fibromyxoid stroma (compare Fig. 5C to A and B). Still, at the periphery of the SMGs, there is continued persistence of basophilic hypercellularity with occasional inclusion bodies (Fig. 5C).

This "near rescue" of the mCMV-induced pathology with GEF inhibition of EGFR phosphorylation is coincident with a highly significant downstream downregulation of pERK1/2 ($R = 0.48$, $n = 9$, $P < 0.001$) and COX-2 ($R = 0.37$, $n = 9$, $P < 0.0001$) (Fig. 5E–L). The outcome of GEF-inhibition of EGFR activation (Fig. 5) is consistent with prior observations that sensitivity to GEF inhibition in wild-type EGFR is dependent upon a significant upregulation of AREG prior to drug exposure (Yonesaka et al., 2008; Hickinson et al., 2009), being 2-fold in mCMV-infected SMGs (Table 1, Fig. 3B, E, K). It is evident from these studies that AREG-mediated EGFR phosphorylation is a critical, perhaps omnibus, constituent of the molecular pathogenesis. Nonetheless, it is not the entirety of it.

Regulation of cell proliferation and apoptosis by signaling pathways is complicated by pathway crosstalk. In this regard, we investigated the possibility that other receptor tyrosine kinases (RTKs) in the EGFR (ErbB1) family and otherwise might be activated

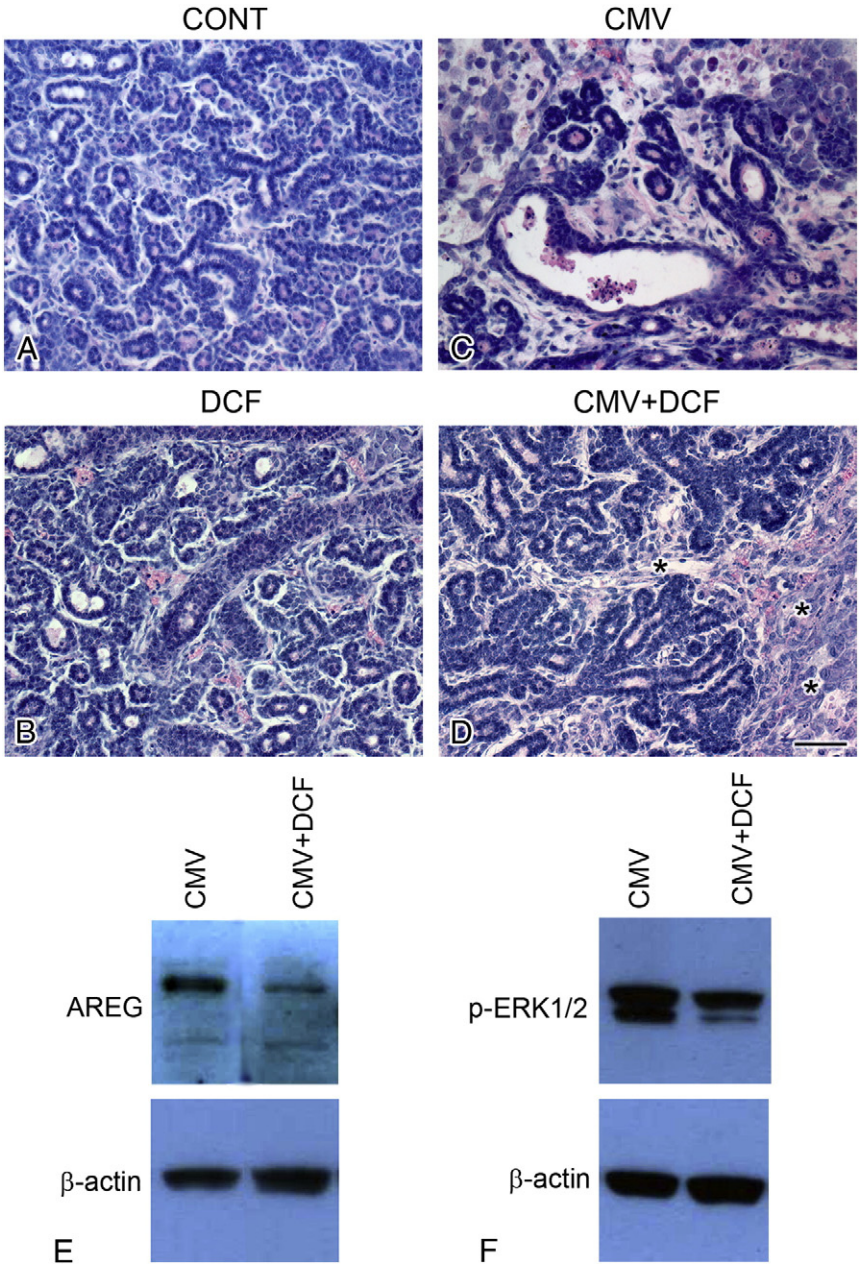

Fig. 4. DCF treatment of mCMV-infected NB + 6 SMGs. A–D. DCF treatment ameliorates CMV-induced histopathology. A. Control NB + 6 SMG. B. NB + 6 SMG treated with 1 μM DCF exhibits a phenotype similar to that seen in control (compare B to A). C. mCMV-infected NB + 6 SMGs are characterized by abnormally large, dilated lumina, decreased branched ductal and acinar epithelia and cytomegalic, hypercellular stroma. D. In mCMV-infected NB + 6 SMGs treated with 1 μM DCF (CMV + DCF), there is considerable "rescue" of the viral-induced pathology (compare D to C). CMV + DCF SMGs are characterized by a substantial increase in ductal and acinar epithelia, with normal-sized lumen being seen. Although the stroma is much improved in appearance, there still remains a smaller, but widespread, amount of basophilic hypercellularity (*). Bar scale: 30 μm. E, F. Western blot analysis demonstrates a significant decrease in AREG (E) and p-ERK1/2 (F) protein expression in DCF-treated, mCMV-infected SMGs compared to mCMV-infected SMGs. Bar scale: A–D, 40 μm.

in mCMV-infected SMGs. NB mouse SMGs were cultured with or without mCMV infection as previously described. Extracted protein from infected and control SMGs was assayed using a phospho-receptor tyrosine kinase array designed to simultaneously detect the relative phosphorylation of 39 different RTKs (Fig. 6). mCMV-induced differences in activation (phosphorylation) is consistently detected in only 3 RTKs as compared to controls (Fig. 6A, B): EGFR (ErbB1) ($R = 3.70$, $n = 4$, $P < 0.05$); ErbB2 ($R = 4.14$, $n = 4$, $P < 0.01$); ErbB3 ($R = 1.82$; $n = 4$, $P < 0.001$). EGFR (ErbB1), ErbB2, and ErbB3, along with ErbB4, are a family of structurally-related RTKs; overactivation of one or more of these family members is associated with tumorigenesis (Hynes et al., 2001; Holbro et al., 2003). Since all three overactivated ErbB receptors have a common intracellular tyrosine kinase domain, we subsequently assayed NB mouse SMGs that were mCMV-infected and cultured with or without GEF (Fig. 6C). GEF treatment of mCMV-infected SMGs downregulates phosphorylation to control levels or below in all three RTKs (compare Fig. 6C to B): EGFR ($R = 0.36$, $n = 4$, $P < 0.01$); ErbB2 ($R = 0.19$, $n = 4$, $P < 0.0001$); ErbB3 ($R = 0.41$, $n = 4$, $P < 0.0001$). Significantly reduced tyrosine phosphorylation by GEF of EGFR, ErbB2 and ErbB3 has recently been reported elsewhere (Djerf et al., 2009). That significant upregulated activation of other RTKs was not detected was surprising and not helpful in solving the enigma of GEF's less than complete rescue of mCMV-induced pathology.

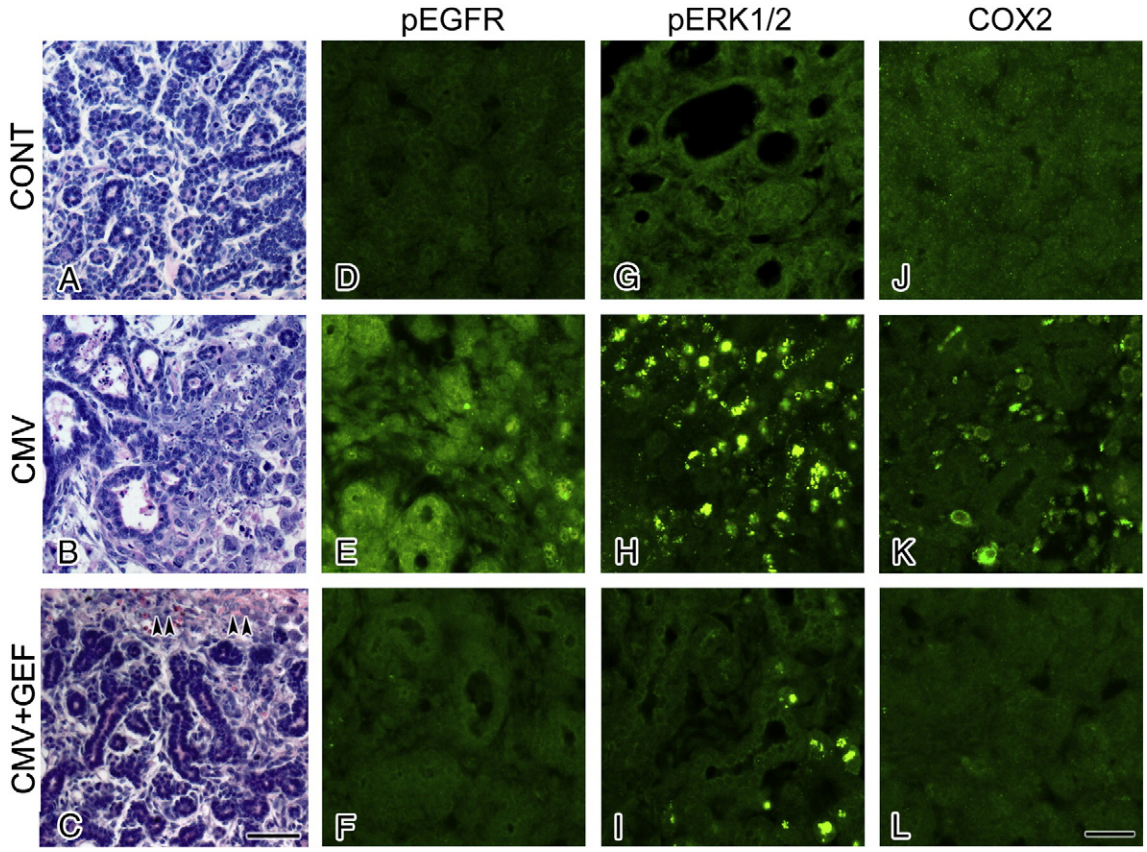

Fig. 5. Gefitinib treatment of CMV-infected NB + 6 SMGs. A–C. GEF treatment ameliorates CMV-induced histopathology. A. Untreated control NB + 6 SMG. B. mCMV-infected NB + 6 SMG exhibits decreased epithelial branching, enlarged lumina, and hypercellular, frequently transformed, stromal cells. C. In mCMV-infected SMGs treated with 10 μM GEF (CMV + GEF), there is considerable "rescue" of the viral-induced pathology, resulting in an epithelial phenotype resembling control SMGs and the presence of normally-appearing fibromyxoid stroma (compare C to B). However, there is continued persistence of basophilic hypercellularity with occasional inclusion bodies at the periphery of the GEF treated gland (arrowheads). D–L. Distribution of phospho-EGFR (pEGFR), phospho-ERK 1/2 (pERK) and COX-2 immunostaining in control (D, G, J), mCMV-infected (E, H, K) and GEF-treated, mCMV-infected (F, I, L) SMGs. D–F. pEGFR localization. GEF treated, mCMV-infected SMGs exhibit a notable decrease in immunodetectable pEGFR compared to mCMV-infected glands (compare F to E); this expression is similar to that seen in control glands (compare F to D). . G–I. pERK1/2 localization. With GEF treatment, there is a marked decrease in immunodetectable p-ERK1/2 compared to mCMV-infected glands (compare I to H). J–L. COX-2 localization. GEF-treated, mCMV-infected SMGs exhibit a marked decrease of immunodetectable COX-2 compared to mCMV-infected SMGs (compare L to K); COX-2 protein expression is similar to that seen in controls (compare L to J). Bar scale: : A–C, 40 μm; D–L, 15 μm.

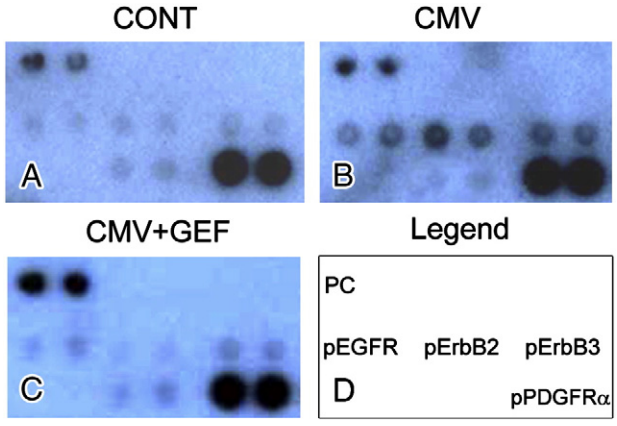

Fig. 6. Expression of activated RTKs in control, mCMV-infected and GEF-treated, mCMV-infected SMGs. We used a phospho-receptor tyrosine kinase array (R & D Systems) designed to simultaneously detect the relative phosphorylation of 39 different receptor tyrosine kinases (RTKs). mCMV infection significantly upregulated phosphorylation in only 3 RTKs compared to controls, pEGFR, pErbB2, and pErbB3 (compare B to A); while uniformly strong, there were no differences in pPDGFRα expression . In CMV + GEF SMG, the expression of activated RTKs is restored to that seen in control SMGs (compare C to A). PC, positive control.

ERK1/2 inhibition

The binding of AREG to the extracellular domain of EGFR (ErbB1) results in receptor homodimerization or heterodimerization with other ErbBs, tyrosine autophosphorylation, the recruitment of the GRB2/SOS signaling complex, GTP-loading of the proximate Ras, and subsequent activation of Raf kinase and a phosphorylation cascade from MEK 1/2 to ERK 1/2. The downstream targets of activated ERK1/2 include ELK1, c-Myc, and other nuclear transcription factors.

As noted above, phosphorylated ERK is increased 2-fold in mCMV-infected SMGs compared to uninfected control SMGs (Table 1; Fig. 3C, F, L). Though this is coincident with a 2-fold increase in phosphorylated EGFR, there may be other pathways that lead to ERK1/2 activation, and this could explain GEF's less than complete rescue of mCMV-induced pathology. For example, previously in mCMV-infected fetal SMGs, we identified a dramatic upregulation of the IL-6 pathway (Melnick et al., 2006). Assaying IL-6 in mCMV-infected NB SMGs by qRT-PCR reveals a 90-fold increase ($R = 90.1$, $n = 9$, $P < 0.01$) in IL-6 transcripts as compared to uninfected, control NB SMGs. Albeit that IL-6 signaling can be achieved through other pathways (e.g. JAK/STAT and PI3K/Akt), the Ras-mediated ERK pathway is a major effector of IL-6/IL-6R/GP130 activation. Thus, we hypothesized that ERK activation by pathways other than EGFR accounted for the incomplete rescue of mCMV-induced pathology. We tested this hypothesis by direct inhibition of

ERK activation using U0126, a small molecule inhibitor of MEK-mediated ERK phosphorylation (e.g. see Sturm et al., 2010).

NB SMGs were infected with 1×10^5 PFU/ml mCMV for 24 h in the presence or absence of 50 μM U0126 and then cultured in control medium with or without U0126 and maintained for a total of 6 days. Controls consisted of SMGs cultured in control medium or control medium + U0126 for the entire 6 day period. SMGs were collected on day 6 (NB + 6) for histologic and immunolocalization studies. mCMV-infected NB + 6 SMGs treated with 50 μM U0126 exhibit complete rescue of CMV-induced pathology (compare Fig. 7C to A, B). Treated SMGs have a substantial increase in ductal and acinar epithelia with normal-sized lumina, surrounded by normal appearing, compacted mesenchyme (Fig. 7C). This morphology is indistinguishable from that seen in control SMGs (compare Fig. 7C to A) and markedly differs from the histopathology seen in untreated, mCMV-infected SMGs (compare Fig. 7C to B). Coincident with the U0126-mediated dramatic change in histologic phenotype, there is a dramatic decrease in the SMG tissue expression of pERK1/2 protein (compare Fig. 7F to E) and a return of normal patterns of cell proliferation (compare Fig. 7I to G, H). Taken together, these results indicate that upregulation of ERK1/2 activation is critical to the initial mCMV-induced epithelial dysplasia, stromal metaplasia, and other early characteristics of mouse SMG tumor formation.

Discussion

Using genomic, proteomic, histologic and other related methodologies, the objective of systems genetics is to elucidate how genetic information is integrated, coordinated, and ultimately transmitted through molecular, cellular, and physiologic networks to permit emergent properties of complex disease (Nadeau and Dudley, 2011). Thus, the central interest of systems genetics is on networks of interaction between genes and phenotypes. Though scores of genes may at first seem to be critical to such interactions, they and their cognate networks can be prioritized using unbiased learning methods such as probabilistic neural network analysis (Melnick et al., 2001, 2006, 2009; Jaskoll et al., 2010). A priori predictions that follow from a high priority network model can be tested in the usual manner (gene mutations, small molecule inhibitors, environmental exposures). Recognizing the reality of crosstalk between signaling pathways, it is likely that a network model will grow in complexity with investigation. Nonetheless, it will provide an informed and objective strategy to identify therapeutic targets to ameliorate and prevent disease.

In the present study, we investigated a network (Fig. 2A) previously suggested in studies of CMV-induced fetal SMG dysplasia (Melnick et al., 2006), hypothesizing that this network would be

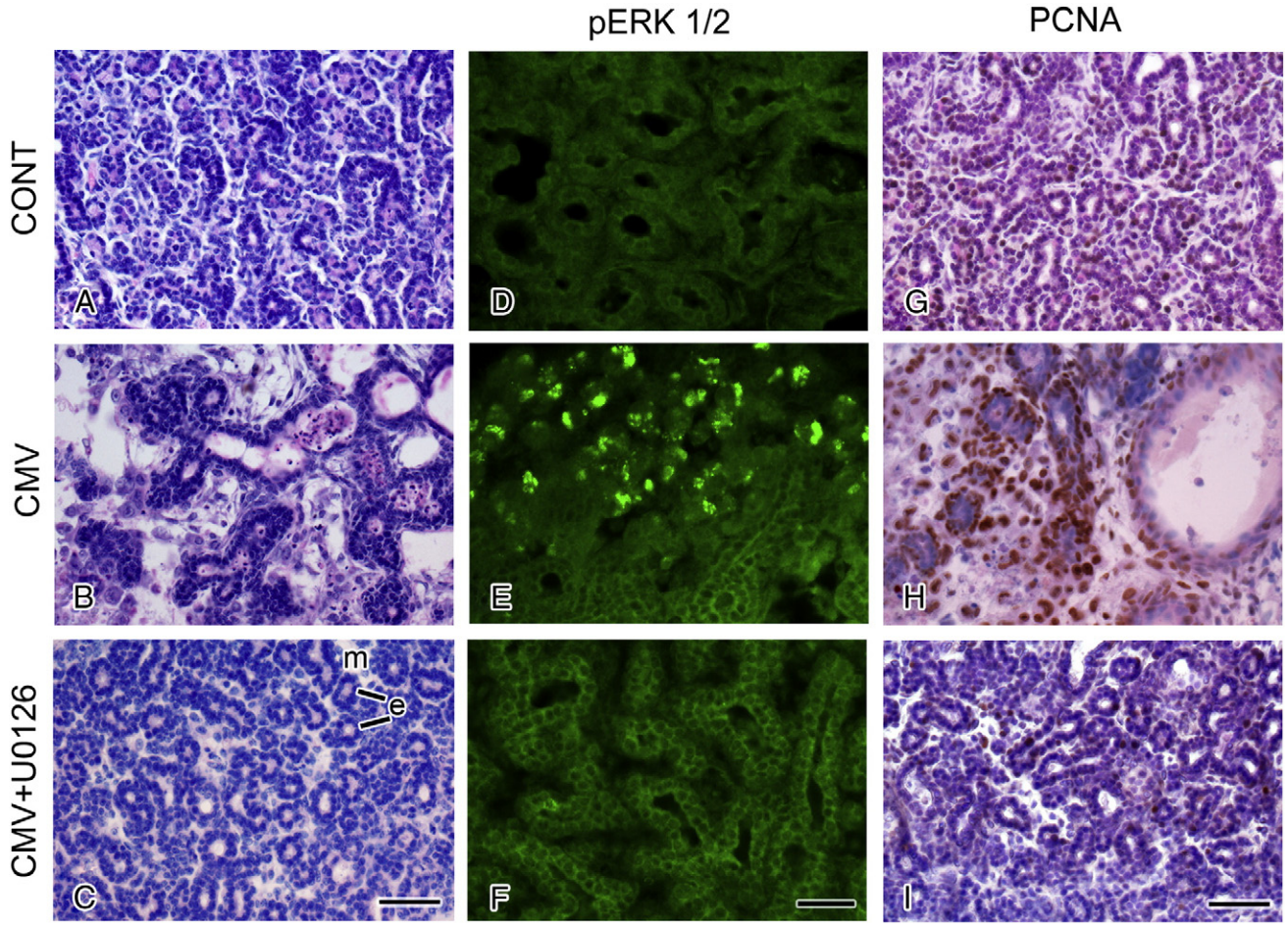

Fig. 7. U0126 treatment of CMV-infected NB + 6 SMGs. A–C. U0126 treatment rescues the CMV-induced histopathology. A. Untreated control NB + 6 SMGs. B. mCMV-infected NB + 6 SMGs. C. In mCMV-infected SMGs treated with 50 μM U0126 (CMV + U0126), a "rescue" of the viral-induced pathology is seen. U0126-treated SMGs exhibit a substantial increase in ductal and acinar epithelia (e) surrounded by normal appearing, compacted mesenchyme (m) (compare C to B). This phenotype is similar to that seen in control SMGs (compare C to A) and notably different from untreated, mCMV-infected SMG (compare C to B). D–F. Distribution of phospho-ERK1/2 (pERK) immunostaining in control (D), mCMV-infected (E) and U0126-treated, mCMV-infected (F) SMGs. U0126 treatment of mCMV-infected SMGs results in a marked decrease in activated ERK1/2 treatment compared to mCMV-infected glands (compare F to E). Bar scale: 30 μm. G–I. Distribution of PCNA-positive nuclei. U0126 treatment results in a cell-specific pattern of PCNA-positive nuclei resembling that seen in controls (compare I to G); This markedly differs from the untreated, mCMV-infected glands in which PCNA-positive nuclei are primarily found in the cytomegalic, abnormal stromal cells (compare I to H). Bar scale: A–C, 40 μm; D–F, 15 μm; G–I, 40 μm.

highly relevant to postnatal CMV-induced tumorigenesis (Jaskoll et al., 2011). In support of this model, we were able to generate an unbiased optimization algorithm that permits the transcript levels of only four genes (COX-2, AREG, ERK1, PCNA) to classify a SMG organ as either CMV-infected or not with 100% sensitivity and 100% specificity (Fig. 2B). The objective of this study was to use small molecule inhibitors to target several key steps in this COX-2/AREG/EGFR/ERK autocrine loop (Figs. 2A, 4, 5, 7), and in this way ameliorate pathology.

Cyclooxygenase-2 (COX-2) overexpression is known to play a key role in early and intermediate stages of tumorigenesis in head and neck squamous cell carcinoma and that levels of COX-2 expression are a statistically significant predictor of survival (Saba et al., 2009). As demonstrated in other solid epithelial tumors (e.g. mammary gland, gastrointestinal), COX-2 overexpression is the initiating catalyst of the COX-2/AREG/EGFR/ERK autocrine loop (Subbaramaiah et al., 2008; Oshima et al., 2011).

In the present study, we find that CMV-induced COX-2 overexpression is also coincident with overexpression of AREG, activated EGFR, and activated ERK1/2 (pERK) (Figs. 3 and 5). Here we also demonstrate that COX-2 inhibition of CMV-infected SMGs by diclofenac sodium fully rescues SMG epithelial structures and partially rescues the stroma. As expected, there is a significant decline in AREG and phospho-ERK1/2 (pERK). It has been suggested that COX-2 inhibition may be an effective strategy for preventing epithelial tumors (Saba et al., 2009; Oshima et al., 2011). Our results would support this. However, it is now quite apparent that COX inhibitors are associated with a very high risk of myocardial infarction, stroke, and cardiovascular death (Trelle et al., 2011). Thus, COX-2 inhibitors would have limited, if any, usefulness as an anti-CMV therapy.

It has been known for nearly two decades that the overexpression of AREG induces epithelial hyperplasia and tumorigenesis in a wide variety of tissues in vivo (Kenney et al., 1996; Willmarth and Ethier, 2006), and that it effects this pathology through a self-sustaining autocrine loop that includes AREG binding to and activation of epidermal growth factor receptor (EGFR) (Willmarth and Ethier, 2006). It is also well known that AREG and EGFR (ErbB1) are co-overexpressed in human tumors (e.g. Lejeune et al., 1993). Recent studies suggest that AREG alters EGFR internalization and degradation in a way that favors accumulation of EGFR at the cell surface and ultimately leads to changes in EGFR (Willmarth et al., 2009). This is consistent with our finding of a significant ($P<0.01$) downregulation of EGFR transcript in mCMV-infected NB SMGs (data not shown), a consequence of negative feedback.

As in salivary gland and other head and neck tumors (Agulnik et al. 2007; Locati et al., 2009; Rogers et al., 2009), here we demonstrate that CMV-induced SMG tumorigenesis (Fig. 1) is also associated with overexpression of activated EGFR (ErbB1) and pERK1/2 (Fig. 5). Targeted inhibition of EGFR phosphorylation by gefitinib (GEF), an ErbB tyrosine kinase inhibitor, results in total rescue of SMG epithelia, near rescue of SMG stroma, and levels of pEGFR, pERK1/2 and COX-2 normally found in uninfected (control) NB SMGs (Fig. 5). Recent studies suggest that combined treatment with COX-2 and EGFR inhibitors would be synergistic (Oshima et al., 2011). We found this is not the case in our model system (data not shown).

In addition to upregulated EGFR (ErbB1) phosphorylation, mCMV-infected NB SMGs also exhibit significant upregulation of phosphorylated family members ErbB2 and ErbB3 (Fig. 6). This has been seen in a variety of human malignancies, including salivary gland tumors, head and neck squamous cell carcinoma, breast tumors, and melanoma (Agulnik et al., 2007; D'Alessio et al., 2010; Djerf et al., 2009; Rogers et al., 2009). We also find that in our mCMV-infected postnatal mouse tumor model, gefitinib (GEF) significantly reduces tyrosine phosphorylation of all three ErbBs (B1, B2, B3). This has been demonstrated previously in malignant melanoma and breast cancer cells (D'Alessio et al., 2010; Djerf et al., 2009); interestingly, concomitant upregulation of EGFR and ErbB2 phosphorylation appears to influence sensitivity to GEF treatment in head and neck squamous carcinoma cells (Rogers et al., 2009).

GEF inhibition of ErbB phosphorylation is associated with concomitant decline of ERK, Akt and STAT 3 phosphorylation (Fig. 5; Piechocki et al., 2008; Djerf et al., 2009). All three signaling pathways are downstream of ErbB phosphorylation (Hynes et al., 2001). This raises the question of the relative importance of the ERK, Akt, and STAT 3 pathways to the associated histopathologies. Regarding this, we find that inhibition of MEK-mediated phosphorylation of ERK results in complete rescue of mCMV-induced pathology (Fig. 7). While these results do not entirely rule out the possibility that Akt and STAT 3 play an ancillary role, they do indicate that the upregulation of ERK phosphorylation is necessary for initial mCMV-induced postnatal SMG pathogenesis.

Human CMV (hCMV), both active and latent, has a particular tropism for salivary glands (Wagner et al., 1996; Nichols and Boeckh, 2000). In the immunocompromised patient, hCMV is a common cause of opportunistic infections, and subsequent morbidity and mortality (Kim et al., 2010; Mori and Kato, 2010). Thus, there is a critical need to develop more effective and less toxic anti-CMV therapies (Andrei et al., 2008). The experimental results reported here indicate that ErbB phosphorylation and downstream signaling are highly relevant targets for drug therapy. This may be all the more important because recent studies demonstrate that EGFR (ErbB1) signaling is essential to mediating hCMV entry into monocytes and ultimately promotion of hematogenous dissemination of hCMV to multiple organ systems (Chan et al., 2009, 2010).

List of abbreviations

AREG	amphiregulin
CMV	cytomegalovirus
CONT	control
DCF	diclofeneac sodium salt
GEF	gefitinib
hCMV	human cytomegalovirus
mCMV	mouse cytomegalovirus
NB	newborn
PCNA	proliferating cell nuclear antigen
PFU	plaque forming units
PNN	Probabilistic neural network analysis
qRT-PCR	quantitative RT-PCR
RTK	receptor tyrosine kinase
SMG	salivary gland

Conflict of interests

The authors declare that there are no conflicts of interest.

Acknowledgments

We would like to thank Dr. Edward Mocarski for his generous gift of mCMV. This research was supported by NIH grants RO1 DE014535 and R21 DC010424 (TJ/MM).

References

Agulnik, M., et al., 2007. Phase II study of lapatinib in recurrent or metastatic epidermal growth factor receptor and/or erbB2 expressing adenoid cystic carcinoma and non adenoid cystic carcinoma malignant tumors of the salivary glands. J. Clin. Oncol. 25, 3978–3984.

Andrei, G., et al., 2008. Novel inhibitors of human CMV. Curr. Opin. Investig. Drugs 9, 132–145.

Bai, Y., et al., 2008. Effective inhibition in animals of viral pathogenesis by a ribozyme derived from RNase P catalytic RNA. Proc. Natl. Acad. Sci. U. S. A. 105, 10919–10924.

Chan, G., et al., 2009. Activation of EGFR on monocytes is required for human cytomegalovirus entry and mediates cellular motility. Proc. Natl. Acad. Sci. 106, 22369–22374.
Chan, G., et al., 2010. PI3K-dependent upregulation of Mcl-1 by human cytomegalovirus is mediated by epidermal growth factor receptor and inhibits apoptosis in short-lived monocytes. J. Immunol. 184, 3213–3222.
Cheeran, M.C., et al., 2009. Neuropathogenesis of congenital cytomegalovirus infection: disease mechanisms and prospects for intervention. Clin. Microbiol. Rev. 22, 99–126.
Chen, C. (Ed.), 1996. Fuzzy Logic and Neural Network Handbook. McGraw-Hill, New York.
Correia-Silva Jde, F., et al., 2007. Cytomegalovirus shedding in the oral cavity of allogeneic haematopoietic stem cell transplant patients. Oral Dis. 13, 163–169.
Correia-Silva, J.F., et al., 2010. Saliva as a source of HCMV DNA in allogeneic stem cell transplantation patients. Oral Dis. 16, 210–216.
D'Alessio, A., et al., 2010. Effects of the combined blockade of EGFR and ErbB-2 on signal transduction and regulation of cell cycle regulatory proteins in breast cancer cells. Breast Cancer Res. Treat. 123, 387–396.
Djerf, E.A., et al., 2009. ErbB receptor tyrosine kinases contribute to proliferation of malignant melanoma cells: inhibition by gefitinub. Melanoma Res. 19, 156–166.
Favoni, R.E., et al., 2010. Gefitinib targets EGFR dimerization and ERK1/2 phosphorylation to inhibit pleural mesothelioma cell proliferation. Curr. Cancer Drug Targets 10, 176–191.
Goldberg, D.E., 1989. Genetics algorithms in search, optimization, and machine learning. Addison-Wesley, Reading, Mass.
Hickinson, D.M., et al., 2009. Identification of biomarkers in human head and neck tumor cell lines that predict for *in vitro* sensitivity to gefitinib. CTS J. 2, 183–192.
Holbro, T., et al., 2003. The ErbB receptors and their role in cancer progression. Exp. Cell Res. 284.
Holland, J.H., 1975. Adaptation in Natural and Artificial Systems. University of Michigan Press, Ann Arbor.
Hynes, N.E., et al., 2001. The ErbB receptor tyrosine family as signal integrators. Endocr. Relat. Cancer 8, 151–159.
Jaskoll, T., et al., 2008a. Cytomegalovirus inhibition of embryonic mouse tooth development: a model of the human amelogenesis imperfecta phenocopy. Arch. Oral Biol. 53, 405–415.
Jaskoll, T., et al., 2008b. Cytomegalovirus induces abnormal chondrogenesis and osteogenesis during embryonic mandibular development. BMC Dev. Biol. 8, 33.
Jaskoll, T., et al., 2010. Cytomegalovirus induces stage-dependent enamel defects and misexpression of amelogenin, enamelin and dentin sialophosphoprotein in developing mouse molars. Cells Tissues Organs 192, 221–239.
Jaskoll, T., et al., 2011. CRTC1 expression during normal and abnormal salivary gland development supports a precursor cell origin for mucoepidermoid cancer. Gene Expr. Patterns 11, 57–63.
Kasman, L.M., et al., 2009. A mouse model linking viral hepatitis and salivary gland dysfunction. Oral Dis. 15, 587–595.
Kenney, N.J., et al., 1996. Induction of ductal morphogenesis and lobular hyperplasia by amphiregulin in the mouse mammary gland. Cell Growth Differ. 7, 1769–1781.
Kim, J.M., et al., 2010. The risk factors for cytomegalovirus syndrome and tissue-invasive cytomegalovirus disease in liver transplant recipients who have cytomegalovirus antigenemia. Transplant. Proc. 42, 890–894.
Krmpotic, A., et al., 2003. Pathogenesis of murine cytomegalovirus infection. Microbes Infect. 5, 1263–1277.
Lagenaur, L.A., et al., 1994. Structure and function of the murine cytomegalovirus *sgg1* gene: a determinant of viral growth in salivary gland acinar cells. J. Virol. 68, 7717–7727.
LeJeune, S., et al., 1993. Amphiregulin, epidermal growth factor receptor, and estrogen receptor expression in human primary breast cancer. Cancer Res. 53, 3597–3602.
Liu, M., et al., 2007. EGFR signaling is required for TGF-β1-mediated COX-2 induction in human bronchial epithelial cells. Am. J. Respir. Cell Mol. Biol. 37, 578–588.
Locati, L.D., et al., 2009. Cetuximab in recurrent and/or metastatic salivary gland carcinomas: a phase II study. Oral Oncol. 45, 574–578.
Lurje, G., Lenz, H.J., 2009. EGFR signaling and drug discovery. Oncology 77, 400–410.
Melnick, M., et al., 2001. The functional genomic response of developing embryonic submandibular glands to NF-kappa B inhibition. BMC Dev. Biol. 1, 15.
Melnick, M., et al., 2006. Cytomegalovirus-induced embryopathology: mouse submandibular salivary gland epithelial-mesenchymal ontogeny as a model. BMC Dev. Biol. 6, 42.
Melnick, M., et al., 2009. Salivary gland branching morphogenesis: a quantitative systems analysis of the Eda/Edar/NFkappaB paradigm. BMC Dev. Biol. 9.
Mori, T., Kato, J., 2010. Cytomegalovirus infection/disease after hematopoietic stem cell transplantation. Int. J. Hematol. 91, 588–595.
Nadeau, J.H., Dudley, A.M., 2011. Systems genetics. Science 331, 1015.
Nichols, W.G., Boeckh, M., 2000. Recent advances in the therapy and prevention of CMV infections. J. Clin. Virol. 16, 25–40.
Oshima, H., et al., 2011. Activation of epidermal growth factor receptor signaling by the prostaglandin E_2 receptor EP4 pathway during gastric tumorigenesis. Cancer Sci. 102, 713–719.
Piechocki, M.P., et al., 2008. Gefitinib prevents cancer progression in mice expressing the activated rat HER2/neu. Int. J. Cancer 122, 1722–1729.
Pilgrim, M.J., et al., 2007. A focused salivary gland infection with attenuated MCMV: an animal model with prevention of pathology associated with systemic MCMV infection. Exp. Mol. Pathol. 82, 269–279.
Reynolds, R.P., et al., 1993. Experimental murine cytomegalovirus infection in severe combined immunodeficient mice. Lab. Anim. Sci. 43, 291–295.
Rogers, S.J., et al., 2009. Detriminants of response to epidermal growth factor receptor tyrosine kinase inhibition in squamous cell carcinoma of the head and neck. J. Pathol. 218, 122–130.
Saba, N.F., et al., 2009. Role of cyclooxygenase-2 in tumor progression and survival of head and neck squamous cell carcinoma. Cancer Prev. Res. 2, 823–829.
Sanchez, V., Spector, D.H., 2008. Subversion of cell cycle regulatory pathways. Curr. Top. Microbiol. Immunol. 325, 243–262.
Schleiss, M., Choo, D., 2006. Mechanisms of congenital cytomegalovirus-induced deafness. Drug Discov. Today 3, 105–113.
Schmader, K., et al., 1995. Mouse cytomegalovirus reactivation in severe combined immune deficient mice after implantation of latently infected salivary gland. J. Infect. Dis. 172, 531–534.
Schwegmann, A., Brombacher, F., 2008. Host-directed drug targeting of factors hijacked by pathogens. Sci. Signal. 1, re8.
Specht, D., 1988. Probabilistic neural network for classification, mapping, or associative memory. Proc. IEEE Int. Conf. Neural Netw. 1, 525–532.
Specht, D., Shapiro, P., 1991. Generalization accuracy of probabilistic neural networks captured with back-propagation networks. Proc. IEEE Int. Joint Conf. Neural Netw. 1, 887–892.
Sturm, O.E., et al., 2010. The mammalian MAPK/ERK pathway exhibits properties of a negative feedback amplifier. Sci. Signal. 3, ra90.
Subbaramaiah, K., et al., 2008. Cyclooxygenase-2-derived prostaglandin E_2 stimulates *Id-1* transcription. J. Biol. Chem. 283, 33955–33968.
Trelle, S., et al., 2011. Cardiovascular safety of non-steroidal anti-inflammatory drugs: network meta-analysis. BMJ 342, c7086.
Wagner, R.P., et al., 1996. AIDS-associated infections in salivary glands: autopsy survey of 60 cases. Clin. Infect. Dis. 22, 369–371.
Willmarth, N.E., Ethier, S.P., 2006. Autocrine and juxtacrine effects of amphiregulin on the proleferative, invasive and migratory properties of normal and neoplastic human mammary epithelial cells. J. Biol. Chem. 281, 37728–37737.
Willmarth, N.E., et al., 2009. Altered EGFR localization and degradation in human breast cancer cells with an amphiregulin/EGFR autocrine loop. Cell. Signal. 21, 212–219.
Yahav, D., et al., 2009. Antiviral prophylaxis in haematological patients: systematic review and meta-analysis. Eur. J. Cancer 45, 3131–3148.
Yonesaka, K., et al., 2008. Autocrine production of amphiregulin predicts sensitivity to both gefitinib and cetuximab in EGFR wild-type cancers. Clin. Cancer Res. 14, 6963–6973.